Research Square

Preprints are preliminary reports that have not undergone peer review.
They should not be considered conclusive, used to inform clinical practice,
or referenced by the media as validated information.

Electrospun Fibers for Colorimetric Detection of Volatile Organic Compounds via Polyfluorene–Quinoxaline Copolymer Photoproperties Change

Jiyoung Boo
Inha University
Jaedoo Nam
Kyungpook National University
Seongwan Bae
Inha University
Jae Yong Lee
Kyungpook National University
Jinho Choi
jinho.choi.acad@gmail.com
University of Michigan https://orcid.org/0009-0007-5464-8338
Dong Hyuk Park
Inha University
Jongho Kim
Kyungpook National University

Research Article

Keywords: Electrospinning, Conjugated polymer nanofiber, Donor-acceptor copolymer, Intermolecular charge transfer, Colorimetric gas sensing

Posted Date: April 13th, 2026

DOI: https://doi.org/10.21203/rs.3.rs-9158955/v1

License: This work is licensed under a Creative Commons Attribution 4.0 International License.
Read Full License

Version of Record: A version of this preprint was published at Korean Journal of Chemical Engineering on August 3rd, 2026. See the published version at https://doi.org/10.1007/s11814-026-00795-z.

Electrospun Fibers for Colorimetric Detection of Volatile Organic Compounds via Polyfluorene–Quinoxaline Copolymer Photoproperties Change

Jiyoung Boo[1,†] · Jaedoo Nam[2,†] · Seongwan Bae[1,†] · Jae Yong Lee[2] · Jinho Choi[3,*] · Dong Hyuk Park[1,*] · Jongho Kim[2,*]

[1]*Department of Chemical Engineering, Inha University, Incheon 22212, Republic of Korea*

[2]*Department of Textile System Engineering, Kyungpook National University, Daegu 41566, Republic of Korea*

[3]*Department of Materials Science and Engineering, University of Michigan, Ann Arbor, Michigan 48109, USA*

[†]*These authors contributed equally to this work.*

ABSTRACT

We report a volatile organic compound (VOC) sensing platform based on electrospun nanofibers of a single-component PFO–quinoxaline donor–acceptor copolymer, in which donor and acceptor units are covalently integrated within one conjugated chain. Unlike multicomponent systems governed by intermolecular geometry, this design enables VOC-responsive modulation of intrinsically defined excited-state energy flow and charge-transfer photophysics. By tuning the PFO/QX composition, the copolymer showed systematic changes in emission color and lifetime, reflecting composition-dependent donor-to-acceptor interactions. When processed into nanoporous electrospun nanofibers, these chain-level photophysical responses became strongly amplified by enhanced analyte accessibility and nonequilibrium chain packing. In particular, the 95:5 composition exhibited distinct blue-to-green emission changes, red-shifted photoluminescence, and shortened fluorescence lifetimes upon exposure to chloroform and tetrahydrofuran vapors, whereas spin-coated films showed only minor responses. These results show that VOCs can directly perturb the photophysical balance within a molecularly integrated donor–acceptor copolymer and demonstrate a simple strategy for visually readable optical gas sensing based on single-chain electronic structure and nanofiber morphology.

Keywords

Electrospinning · Conjugated polymer nanofiber · Donor-acceptor copolymer · Intermolecular charge transfer · Colorimetric gas sensing

(corresponding author email: sci.jongho@knu.ac.kr · donghyuk@inha.ac.kr · jinhoc@umich.edu)

Introduction

Volatile organic compounds (VOCs) remain a persistent concern in laboratory and industrial environments due to their impact on human health and environmental safety [1, 2]. In many practical scenarios, rapid and interpretable detection is as critical as achieving low detection limits [3, 4]. Colorimetric optical sensing is particularly attractive because it enables immediate visual readout under ambient conditions with minimal power consumption and without complex instrumentation [5-7]. However, the primary challenge is not sensitivity alone but achieving reliable gas discrimination while preserving structural simplicity [8]. Sensor arrays combined with pattern recognition algorithms have been widely used to enhance selectivity in VOC sensing systems [9]. However, such approaches often increase system complexity and reduce the operational simplicity of colorimetric sensors [10]. This trade-off motivates simplified sensing concepts capable of producing gas-dependent optical signatures within a single, visually interpretable material system.

Conjugated polymers offer a promising route toward such minimal platforms because their delocalized π-electron systems and excitonic processes are highly responsive to local environmental changes, including polarity, free volume, and chain packing [11-13]. This sensitivity can translate subtle vapor–material interactions into amplified optical responses [14]. At the same time, conjugated polymer photophysics is often strongly morphology-dependent, with optical behavior varying substantially across solution, thin-film, and fibrous states [9, 15, 16]. Such variability complicates mechanistic interpretation and can limit reproducibility across device formats. A central challenge, therefore, is to harness polymer-based optical sensitivity within a framework that remains mechanistically defined and robust in practical sensing architectures [17].

Electrospun colorimetric systems have frequently employed Förster resonance energy transfer (FRET) as a convenient radiometric readout [9, 18, 19]. However, FRET-based sensing depends critically on nanoscale donor–acceptor separation, molecular orientation, and spatial distribution—parameters that are difficult to control in nonequilibrium electrospun nanofibers [20]. Rapid solvent evaporation and heterogeneous chain packing can generate structural inhomogeneity and defect-like microenvironments that distort energy-transfer efficiencies and obscure interpretation [21]. These

considerations highlight the need for alternative approaches in which the sensing response is governed primarily by intrinsic, molecularly defined photophysical pathways rather than fragile geometric constraints.

Here, we present a simplified colorimetric VOC sensing platform based on a single donor–acceptor (D–A) copolymer integrated into an electrospun nanofiber architecture. The copolymer design provides an intrinsic route for vapor-responsive modulation of excited-state energy flow, while the nanofiber morphology enhances analyte accessibility and optical contrast through high surface-to-volume ratios and interconnected porosity. By correlating spectral evolution with excited-state dynamics, we establish a photophysically interpretable basis for visually readable VOC detection. Overall, this work demonstrates that coupling molecularly engineered D–A photophysics with nanofiber morphology can enable a structurally simple yet effective strategy for VOC-responsive optical sensing.

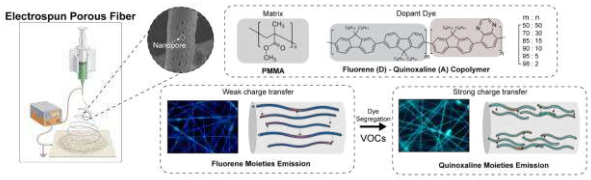


Fig.1 Schematic illustration of the colorimetric gas-sensing platform on donor-acceptor PFO@QX nanofibers

Experimental

Chemicals and Materials

9,9-Dioctyl-2,7-dibromofluorene (M1), tetrakis(triphenylphosphine)-palladium(0), and bromobenzene (M4) were purchased from Sigma-Aldrich. 9,9-Dioctylfluorene-2,7-diboronic acid bis(1,3-propanediol) ester (M2) was purchased from Sigma-Aldrich, and 5,8-dibromoquinoxaline (M3) was purchased from AmBeed. 4,4,5,5-Tetramethyl-2-phenyl-1,3,2-dioxaborolane (M5) was purchased from BLD Pharm. All chemicals were used as received without further purification.

Characterization

^{1}H and ^{13}C NMR spectra were recorded on a Bruker Avance Neo 500 spectrometer operating at 500 MHz. Gel permeation chromatography (GPC) measurements were performed using a Waters Alliance e2695 system with chloroform as the eluent. UV–vis absorption spectra were recorded on a JASCO V-770 UV–visible/NIR spectrophotometer. Photoluminescence (PL) spectra were recorded using a Varian Cary Eclipse spectrophotometer and spectrometer (SR-303I-B, Andor) coupled with a CCD detector (GF-033C-IRF, Allied Vision). Time-resolved photoluminescence (TR-PL) measurements were carried out using a time-correlated single-photon counting (TCSPC) system to analyze the excited-state decay dynamics. Scanning electron microscopy (SEM) images were obtained using a high-resolution scanning electron microscope (HRSEM).

Synthesis of PFO@QX Copolymer

A series of PFO@QX donor–acceptor copolymers with varying composition ratios (50:50 to 98:2) were synthesized via a Suzuki coupling reaction under identical reaction conditions. The monomer ratios of the fluorene-based donor monomer (M1) and quinoxaline-based acceptor monomer (M3) were systematically adjusted to control the m:n composition, while the diboronic fluorene monomer (M2) was kept constant. The reaction was carried out in a toluene/aqueous K_2CO_3 biphasic system using $Pd(PPh_3)_4$ as a catalyst and Aliquat 336 as a phase-transfer agent under an argon atmosphere. End-capping reactions were performed to quench residual reactive chain ends. The resulting polymers were purified by precipitation and Soxhlet extraction, affording moderate to high yields. Detailed synthetic procedures and characterization data are provided in the Supporting Information.

Fabrication of PFO@QX Nanofibers

Poly(methyl methacrylate) (PMMA) and PFO@QX were separately dissolved in chloroform at concentrations of 100 mg/mL and 1-4 mg/mL, respectively. To remove any undissolved residues, the PFO@QX solution was filtered through a polypropylene syringe filter prior to use. The two solutions were then mixed at a volume ratio of 1:1 (PMMA:PFO@QX, v:v) to prepare the precursor solution

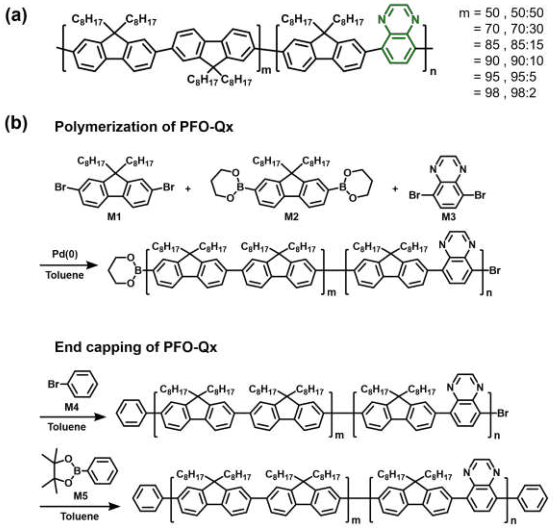
for electrospinning. PFO@QX nanofibers were fabricated via electrospinning using a 10 mL plastic syringe equipped with a 23-gauge stainless steel needle. The needle was connected to a high-voltage power supply, and a constant voltage of 20 kV was applied during electrospinning. The precursor solution was continuously delivered using a syringe pump at a flowrate of 10 μL/min. The distance between the needle and the collector was fixed at 20 cm. To obtain uniform nanofiber mats, glass substrates spin-coated with poly(3,4-ethylenedioxythiophene):polystyrene sulfonate (PEDOT:PSS) were used as collectors.

Solvent Vapor Exposure Procedure

Gas exposure experiments were conducted using a sealed round-bottom flask with a total volume of 250 mL. The electrospun nanofiber film was placed inside the flask prior to vapor exposure. To generate solvent vapors, 200 μL of volatile organic solvents, including chloroform, tetrahydrofuran (THF), ethanol, isopropanol (IPA), and hexane, were injected onto the bottom of the flask without direct contact with the nanofiber film. The injected solvents were allowed to evaporate completely under ambient conditions, and vapor exposure was initiated immediately after complete evaporation. The nanofiber films were exposed to the corresponding solvent vapor for 30 minutes in the sealed environment to ensure sufficient interaction between the vapor molecules and the nanofiber surface.

Results and Discussion

Synthesis and Molecular Properties of PFO@QX Copolymers



Scheme 1 Scheme of the molecular structure and synthetic route of PFO@QX. (a) Molecular structure of the PFO@QX donor-acceptor copolymer, composed of polyfluorene (PFO) donor units and quinoxaline (QX) acceptor units with tunable m:n ratios ranging from 50:50 to 98:2. (b) Polymerization and end-capping reactions of PFO@QX

Scheme 1 shows the molecular structures and synthetic routes of the PFO@QX copolymers. PFO@QX is a donor–acceptor type copolymer composed of polyfluorene (PFO) as an electron-donor unit and quinoxaline (QX) as an electron-acceptor unit, and the copolymer composition ratio (m:n) was controlled from 50:50 to 98:2 by varying the monomer ratios. The copolymers were synthesized via a palladium-catalyzed Suzuki coupling polymerization, followed by end-capping reactions to control the reactivity of the polymer chain ends after completion of the polymerization.

The chemical structures of the copolymers were confirmed by ^{1}H NMR and ^{13}C NMR analyses. The molar composition (m:n) of the copolymers was determined by ^{1}H NMR spectroscopy. For monomer ratios of 50:50, 70:30, 85:15, 90:10, and 95:5, the actual molar compositions were determined to be 71.4:28.6, 84.6:15.4, 90.0:10.0, 92.8:7.2, and 96.9:3.1, respectively. In contrast, for the monomer ratio of 92:8, the signal corresponding to the quinoxaline unit was too weak to allow reliable determination

of the copolymer composition. These results are summarized in **Table 1**. The number-average molecular weight (Mn), weight-average molecular weight (Mw), and polydispersity index (PDI) of the copolymers were evaluated by gel permeation chromatography (GPC), and the molecular weight characteristics as a function of copolymer composition are also summarized in **Table 1**.

Composition		Mn	Mw	PDI	Composition		Mn	Mw	PDI
50:50	(71.4:28.6)	6255	12148	1.94	90:10	(92.8:7.2)	11731	20487	1.74
70:30	(84.6:15.4)	19809	53373	2.69	95:5	(96.9:3.1)	17208	33340	1.94
85:15	(90.0:10.0)	31879	74298	2.33	98:2	-	12488	21097	1.69

Table 1 Actual Molecular Compositions of PFO@QX Copolymers Determined by ^{1}H NMR and Their Molecular Weight Characteristics (Mn, Mw, and PDI) Obtained from GPC Analysis

Photophysical Properties of PFO@QX Copolymers

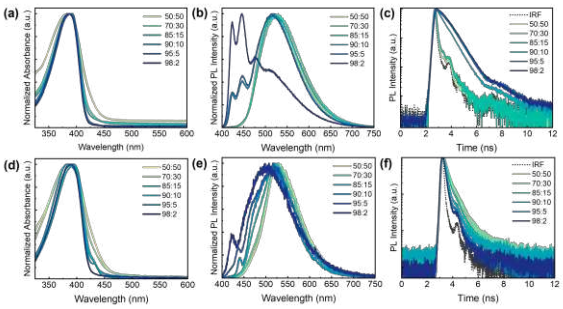


Fig.2 Photophysical properties of PFO@QX copolymers with different composition ratios (m:n). (a) UV–vis absorption spectra, (b) normalized photoluminescence spectra (λ_{ex}:370 nm), and (c) time-resolved photoluminescence decay curve (λ_{ex}:370 nm, λ_{det}:405 nm) of PFO@QX copolymers in chloroform solution, (d) UV–vis absorption spectra, (e) normalized photoluminescence spectra, (f) time-resolved photoluminescence decay curve (λ_{ex}:370 nm, λ_{det}:405 nm) of the corresponding PFO@QX copolymers as spin-coated films

The photophysical properties of the PFO@QX donor–acceptor copolymers with varying composition ratios (m:n) were investigated in solution and as spin-coated films to understand their intrinsic optical characteristics prior to nanofiber fabrication.

In chloroform solution (**Fig. 2a**), all copolymers exhibited a main absorption band centered at 385-390 nm, which can be attributed to the π-π^* transition of the conjugated fluorene backbone [22]. In the film state (**Fig. 2d**), similar absorption features were observed, however, slight broadening toward longer wavelengths became more pronounced with increasing QX content. Compared to solution, this behavior may be related to aggregation-induced chain packing in the solid state, which can stabilize lower-energy electronic states and subtly modify higher-energy absorption features [23].

The photoluminescence (PL) spectra showed a strong composition dependence in both solution (**Fig. 2b**) and film (**Fig. 2e**). In chloroform solution (**Fig. 2b**), the blue emission (400–450 nm), which represents fluorescence from the fluorene component, was quenched as the acceptor ratio in the PFO@QX copolymer increased. In contrast, the green emission (450–650 nm) increased with increasing acceptor ratio. This trend indicates an increasing contribution from lower-energy emissive states associated with donor–acceptor interactions as the acceptor fraction increases [24, 25]. The PL spectra of spin-coated solid thin films showed a clearly different trend from those in solution (**Fig. 2e**). Due to aggregation, all PFO@QX copolymers, regardless of the D/A ratio, exhibited dominant green emission (450–650 nm) with quenched blue emission (400–450 nm). Nevertheless, the green emission appeared more pronounced when the donor concentration was higher rather than lower. These copolymers showed a clear trend of exciton migration from fluorene to quinoxaline as the acceptor concentration increased in the diluted solution state, and this behavior can be enhanced by aggregation. These results confirm that increasing the QX fraction promotes long-wavelength intermolecular charge-transfer (ICT) emission through efficient energy transfer from fluorene to quinoxaline units [25-27].

TRPL measurements in diluted solution (**Fig. 2c**) and spin-coated films (**Fig. 2f**) further revealed composition-dependent excited-state dynamics. These results are summarized in **Table S1.** In solution state, the lifetimes of PFO@QX polymers with varying component ratios showed a decreasing trend

with increasing acceptor fraction at λ_{det} = 405 nm. However, spin-coated films (**Fig. 2f**) exhibited different PL lifetimes, because emission from the donor region was quenched for most compositions, as indicated by the steady-state PL results above. Interestingly, the luminescence lifetime at λ_{det} = 405 nm increased with increasing acceptor ratio. This behavior may be attributed to aggregation-induced modification of the electronic structure in the solid state [28]. Strong interchain interactions can generate new emissive states such as excimer-like or charge-transfer states, which alter excited-state relaxation pathways beyond those present in isolated polymer chains [29]. Such aggregation-driven electronic coupling is known to influence photophysical properties of conjugated polymers by stabilizing lower-energy excited states and modifying radiative and nonradiative decay processes [29, 30]. This trend indicates that QX-rich copolymers possess shorter excited-state lifetimes due to efficient ICT formation and enhanced nonradiative decay pathways. As the QX content decreases, suppression of ICT and restoration of localized fluorene excitons result in longer radiative lifetimes.

Photophysical Properties of Electrospun PFO@QX Nanofibers

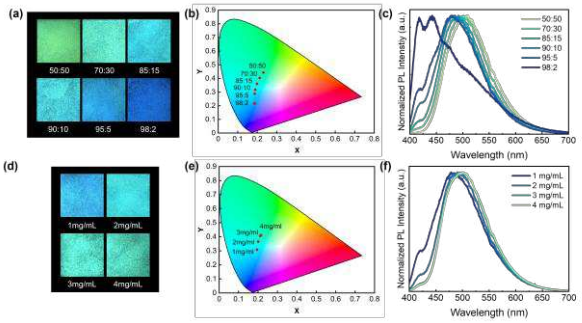


Fig. 3 Photophysical properties of PFO@QX nanofibers as a function of donor-acceptor composition ratio and polymer concentration. (a-c) composition-dependent images under 365nm UV-lamp illumination, CIE 1931 diagram, and normalized photoluminescence spectra (λ_{ex}:370 nm), (d-f) concentration-dependent images under 365nm UV-lamp illumination, CIE 1931 diagram, and normalized photoluminescence spectra (λ_{ex}:370 nm)

Fig. S1 shows the morphological characteristics of the electrospun PFO@QX 95:5 nanofibers. The nanofibers form a randomly oriented and continuously interconnected fibrous network, generating a

highly porous structure with an average fiber diameter of 882.86 nm. Notably, these nanoporous features show an average nanopore diameter of 134.17 nm. This nano-porous nanofiber morphology is expected to facilitate rapid penetration and diffusion of external gas molecules into the polymer matrix, thereby enhancing gas-polymer interactions [31, 32].

The composition-dependent photophysical properties of electrospun PFO@QX nanofibers were systematically investigated by varying the donor–acceptor ratio (m:n) from 50:50 to 98:2 (**Fig. 3a–c**). **Fig. 3a** shows fluorescence images of electrospun PFO@QX nanofibers under 365 nm UV illumination, exhibiting a clear color transition from green to blue as the PFO content increases from 50:50 to 98:2. The CIE diagram (**Fig. 3b**) further confirms the systematic color evolution. The progressive decrease in the y value clearly indicates a transition from green to blue emission. This behavior can be attributed to reduced electron-withdrawing influence of QX at higher PFO fractions, leading to weakened intermolecular charge transfer (ICT) stabilization and restoration of fluorene-centered blue emission [24, 33]. As shown in the normalized PL spectra (**Fig. 3c**), the emission peak gradually blue-shifted with increasing PFO content: 508 nm (50:50), 501 nm (70:30), 492 nm (85:15), 485 nm (90:10), 478 nm (95:5), and 442 nm (98:2). The 50:50 sample exhibited dominant green emission, while intermediate compositions (70:30–90:10) displayed cyan emission, and PFO-rich compositions showed pronounced blue emission. The significant shift to 442 nm for the 98:2 sample indicates near-complete suppression of charge-transfer (CT) emission and recovery of fluorene-dominated π–π^* emission [24].

Fig. 3d–f presents the concentration-dependent photophysical characteristics of electrospun PFO@QX nanofibers. The emission images under 365 nm UV illumination confirm the concentration-dependent color evolution (**Fig. 3d**). They visually show a blue-to-green color transition as concentration increases. This trend is consistent with the CIE diagram (**Fig. 3e**). The increase in the y value from 1 to 3 mg/mL clearly indicates a transition from blue toward green emission, while minimal difference between 3 and 4 mg/mL suggests saturation of the concentration effect. As shown in the normalized PL spectra (**Fig. 3f**), the emission peak gradually red-shifted with increasing polymer concentration from 1 to 4 mg/mL, moving from 478 nm to 501 nm. This shift

indicates a progressive enhancement of lower-energy emissive states at higher concentrations [17]. The higher-energy blue emission was more pronounced at low concentration (1 mg/mL). In contrast, emission near 500 nm became dominant at ≥3 mg/mL, suggesting stabilization of charge-transfer (CT) states with increased polymer packing density.

Fig. S2 and **Table S2** present the time-resolved photoluminescence decay profiles of PFO@QX nanofibers monitored at 405nm. Unlike the clear spectral variations observed in steady-state PL, the lifetime values do not exhibit a pronounced systematic dependence on either donor–acceptor composition or polymer concentration. It suggests that aggregation-induced intermolecular interactions dominate the excited-state dynamics in the solid state [34, 35]. As a result, the emissive states associated with high-energy fluorene transitions are already partially quenched by aggregation-related pathways, leading to comparable decay kinetics among different compositions and concentrations [34]. Therefore, aggregation-induced nonradiative decay appears to dominate the excited-state relaxation process in the nanofiber films, minimizing observable lifetime differences under these detection conditions.

Optimization for Gas-Sensing Conditions of PFO@QX Nanofibers

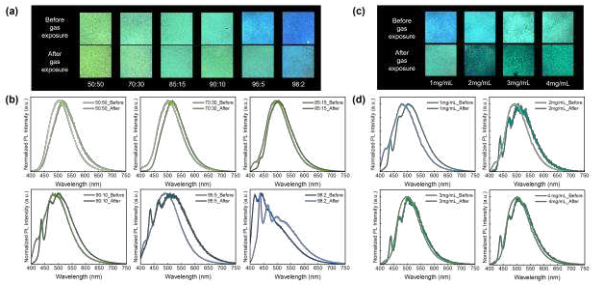


Fig. 4. Responses to gas exposure as a function of donor-acceptor composition (m:n) and polymer concentration. (a) fluorescence images of electrospun membranes with different compositions under UV-lamp irradiation, and (b) corresponding Photoluminescence spectra (λ_{ex}:370 nm). (c) fluorescence images of electrospun membranes with different concentration under UV-lamp irradiation, and (d) corresponding photoluminescence spectra (λ_{ex}:370 nm)

To optimize sensing performance, the effects of copolymer composition and polymer concentration on PL response upon VOC exposure were systematically evaluated. As shown in **Fig. 4a** and **4b**, the PL peak positions after gas exposure shifted to 515, 518, 504, 500, 509, and 436 nm for the 50:50, 70:30, 85:15, 90:10, 95:5, and 98:2 samples, respectively. The corresponding peak shifts were 7, 17, 12, 15, 31, and 6 nm. Among these compositions, the 95:5 copolymer exhibited the largest spectral shift (31 nm) together with the most distinct visual color change from blue to green under UV illumination. 95:5 ratio provides an optimal balance between donor-dominated emission and ICT-sensitive states, enabling amplified spectral modulation upon gas interaction.

The concentration-dependent response (**Fig. 4c,d**) showed gas-induced PL peaks at 505, 503, 502, and 503 nm for 1, 2, 3, and 4 mg/mL samples, corresponding to peak shifts of 27, 13, 2, and 2 nm, respectively. The 1 mg/mL nanofiber exhibited the largest spectral change (27 nm), while higher concentrations showed significantly reduced peak shifts. This trend suggests that lower polymer loading facilitates more efficient gas diffusion and interaction within the porous nanofiber network, leading to stronger modulation of the emissive states. In contrast, denser fiber structures at higher concentrations likely restrict vapor penetration and dampen the optical response.

Based on these results, the 95:5 composition and 1 mg/mL concentration were selected as the optimized sensing conditions, as they produced the most pronounced PL shift and the clearest visually detectable color change upon VOC exposure.

Gas-Responsive Optical Behaviors of PFO@QX Nanofibers

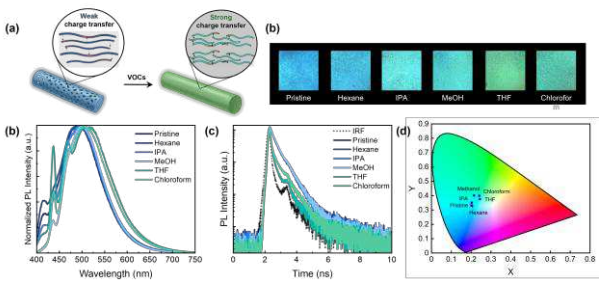


Fig. 5. Gas-responsive optical characteristics of PFO@QX nanofibers upon exposure to various VOCs (Hexane, IPA, Methanol, THF, Chloroform). (a) schematic illustration of the gas-sensing

mechanism, (b) fluorescence images under 365nm UV illumination, (c) corresponding photoluminescence spectra (λ_{ex}:370 nm), (d) time-resolved photoluminescence decay curves (λ_{ex}:370 nm, λ_{det}:405 nm), and (e) CIE 1931 diagram illustrating gas-dependent emission color variations

Fig. 5a schematically illustrates the proposed gas-sensing mechanism of the PFO@QX nanofibers. In the pristine state, the nanofibers exhibit relatively weak charge-transfer (CT) interactions. The emission is mainly governed by fluorene-based π–π* transitions, resulting in blue emission. However, upon VOC infiltration, partial dye segregation within the nanofiber matrix strengthens donor–acceptor interactions between PFO and quinoxaline units. As a result, the emission shifts from blue toward green.

Upon exposure to representative VOC vapors such as hexane, isopropanol (IPA), methanol, tetrahydrofuran (THF), chloroform, the optical properties of the electrospun PFO@QX nanofibers were systematically investigated. As shown in **Fig. 5b**, distinct emission color changes were observed depending on the VOC species. Compared to the pristine blue emission, exposure to chloroform and THF resulted in a clear blue-to-green transition visible to the naked eye. In contrast, methanol, IPA, and hexane induced relatively smaller color variations, maintaining predominantly bluish or slightly cyan emission.

The corresponding PL spectra (**Fig. 5c**) further confirms these gas-dependent optical variations. The pristine nanofibers exhibited a main emission peak at 478 nm. After vapor exposure, the emission maxima shifted to 505 nm (chloroform), 507 nm (THF), 498 nm (MeOH), 501 nm (IPA), and 488 nm (hexane). The largest redshifts were observed for chloroform and THF, which are highly compatible with the PMMA matrix and capable of effectively infiltrating and swelling the nanofibers [36]. Notably, upon exposure to chloroform and THF, a new emission feature emerged around 440 nm. In the PFO@QX copolymer, exposure to polar VOCs led to suppression of the ~420 nm α-phase emission and the appearance of a new ~440 nm β-phase contribution. This behavior is consistent with conventional polyfluorene systems, where VOC vapor infiltration enhances chain mobility and

induces conformational rearrangement from the α-phase (~420 nm) to the more planar β-phase (~440 nm), resulting in red-shifted emission [15, 30]. The observed red-shift of the main emission band can be attributed to the formation of a more planar β-phase structure [30]. Increased planarity enhances π-electron delocalization along the fluorene backbone, facilitating more efficient intermolecular charge transfer to the electron-withdrawing quinoxaline units. The strengthened donor–acceptor interaction stabilizes the excited state, resulting in longer-wavelength emission [24]. Accordingly, the combined effects of β-phase formation and enhanced charge-transfer interactions explain the pronounced red-shift and blue-to-green color transition observed upon exposure to strongly interacting VOCs such as chloroform and THF.

Fig. 5d shows the TRPL decay profiles of PFO@QX nanofibers monitored at the donor emission region (λ_{det}=405 nm). The pristine sample exhibited an average lifetime of 0.32 ns, whereas exposure to chloroform and THF reduced the lifetime to 0.30 ns for both cases. In contrast, weaker-interacting vapors caused little change (hexane: 0.32 ns, IPA: 0.32 ns, methanol: 0.34 ns). The lifetime shortening under chloroform and THF is attributed to enhanced interchain charge transfer from PFO donor segments to QX acceptor segments. As a result, the decay at 405 nm accelerates, consistent with VOC-induced strengthening of donor–acceptor interactions in the nanofiber matrix.

The CIE diagram (**Fig. 5e**) quantitatively supports the visually observed color changes. from blue toward green emission. These results confirm that strongly interacting VOCs induce the most significant electronic and conformational modulation, leading to distinct and quantifiable colorimetric responses.

Upon exposure to VOC vapors, significant changes occur in both the morphology and electronic interactions within the PFO@QX nanofiber matrix. As shown in **Fig. S3**, SEM analysis revealed pronounced nanopore collapse after exposure to chloroform and THF, both of which are highly compatible with the PMMA matrix [9]. This behavior is attributed to solvent-induced swelling and plasticization, leading to reduced porosity and rearrangement of polymer chains [9, 37]. Such structural changes modify the local dielectric environment and intermolecular packing within the

fibers [38]. In contrast, methanol and hexane largely preserved the original nanoporous morphology, indicating weaker interactions with the polymer matrix [39].

As shown in **Fig. S4**, the spin-coated films exhibited negligible spectral changes upon exposure to chloroform and THF, whereas the electrospun nanofibers showed pronounced red-shifts and significant emission modulation under the same conditions. These results highlight the critical role of nanofiber morphology in amplifying gas–polymer interactions. The enhanced response of the nanofibers can be attributed to their high surface-to-volume ratio, nanoporous structure, and nonequilibrium chain packing induced by rapid solvent evaporation during electrospinning [40]. This comparison confirms that the vapor-induced reorganization of nanoporous nanofibers is a key mechanism enabling effective colorimetric gas sensing in the PFO@QX platform.

Conclusion

In this study, we developed a simplified optical gas-sensing platform based on electrospun nanofibers of a PFO–quinoxaline (PFO@QX) donor–acceptor copolymer. The incorporation of quinoxaline units enabled modulation of the electronic structure through intermolecular charge transfer (ICT), resulting in tunable photophysical properties and enhanced responsiveness to volatile organic compounds (VOCs). Electrospinning further introduced nanoporous fiber morphologies with high surface-to-volume ratios and nonequilibrium chain packing, which significantly amplified gas–polymer interactions compared with conventional thin-film systems. Upon exposure to representative VOC vapors such as chloroform and tetrahydrofuran, the PFO@QX nanofibers exhibited distinct emission color changes, spectral shifts, and fluorescence lifetime reductions that were directly observable by the naked eye. These optical responses are attributed primarily to ICT modulation, morphological perturbations of the nanofiber structure, and possible defect-mediated excited-state interactions rather than conventional Förster-type energy transfer mechanisms.

Importantly, this work demonstrates that a structurally simple single-component donor–acceptor copolymer nanofiber system can achieve sensitive and visually distinguishable VOC detection without relying on complex sensor arrays, electronic transducers, or external signal-processing

systems. Beyond sensing performance, the results provide insight into how intermolecular charge transfer, polymer morphology, and defect states collectively govern gas-responsive photophysical behavior in conjugated polymer nanostructures. These findings highlight the potential of conjugated polymer nanofibers as versatile platforms for next-generation optical gas sensors and offer a framework for designing simplified, colorimetric sensing materials based on controlled copolymer electronic structure and nanostructured morphology.

Supplementary Information

The online version contains supplementary material available at https://doi.org/xxx.

Acknowledgements

J.B., S.B., J.C., and D.H.P. acknowledge Korea Foundation for Women in Science, Engineering and Technology (WISET) grant, funded by the Ministry of Science and ICT(MSIT) under the Team Research Program for female engineering students (WISET- 2025-189). J.N., J.Y.L., and J.K. acknowledge the National Research Foundation of Korea (NRF) grant funded by the Korea government (MSIT) (RS-2024-00458149). J.N., J.Y.L., and J.K. acknowledge Basic Science Research Program through the National Research Foundation of Korea (NRF) funded by the Ministry of Education (RS-2025-25402595).

Data availability

The data that support the findings of this study are available from the corresponding author upon reasonable request.

Author information

Jiyoung Boo, Jaedoo Nam and Seongwan Bae have contributed equally to this article as the first author.

Declarations

Conflict of interest The authors declare no competing financial interest.

References

1. X. Zhou, X. Zhou, C. Wang, H. Zhou, Environmental and human health impacts of volatile organic compounds: A perspective review, Chemosphere, 313, 137489 (2023).
2. E. David, V.-C. Niculescu, Volatile organic compounds (VOCs) as environmental pollutants: occurrence and mitigation using nanomaterials, International journal of environmental research and public health, 18, 13147 (2021).

3. B. Zong, S. Wu, Y. Yang, Q. Li, T. Tao, S. Mao, Smart gas sensors: recent developments and future prospective, Nano-Micro Letters, 17, 54 (2025).
4. A.A. Odebowale, A. Abdulghani, A.M. Berhe, D. Somaweera, S. Akter, S. Abdo, K. As' ham, R.M. Saadabad, T.T. Tran, D.P. Bishop, Emerging low detection limit of optically activated gas sensors based on 2D and hybrid nanostructures, Nanomaterials, 14, 1521 (2024).
5. Q. Ye, S. Fan, J. Lao, J. Xu, X. Liu, P. Wu, Research Advances in Conjugated Polymer-Based Optical Sensor Arrays for Early Diagnosis of Clinical Diseases, Polymers, 18, 310 (2026).
6. F.-Q. Yang, L. Ge, Colorimetric sensors: methods and applications, MDPI,pp. 9887. 2023,
7. S. Krishnan, Colorimetric visual sensors for point-of-needs testing, Sensors and Actuators Reports, 4, 100078 (2022).
8. R. Dong, M. Yang, Y. Zuo, L. Liang, H. Xing, X. Duan, S. Chen, Conducting polymers-based gas sensors: Principles, materials, and applications, Sensors, 25, 2724 (2025).
9. H. Im, J. Choi, H. Lee, Z.Y. Al Balushi, D.-H. Park, S. Kim, Colorimetric multigas sensor arrays and an artificial olfactory platform for volatile organic compounds, ACS sensors, 8, 3370–3379 (2023).
10. Z. Li, J.R. Askim, K.S. Suslick, The optoelectronic nose: colorimetric and fluorometric sensor arrays, Chemical reviews, 119, 231–292 (2018).
11. C.S. Sarap, Y. Singh, J.M. Lane, N. Rai, Electronic properties and optical spectra of donor–acceptor conjugated organic polymers, Scientific Reports, 13, 21587 (2023).
12. S. Singhal, P. Yadav, S. Naqvi, S. Gupta, A. Patra, Donor–acceptor–donor copolymers with 3, 4-ethylenedioxythiophene moiety: electropolymerization and effect on optoelectronic and electrochromic properties, ACS omega, 4, 3484–3492 (2019).
13. M. Weis, Organic semiconducting polymers in photonic devices: From fundamental properties to emerging applications, Applied Sciences, 15, 4028 (2025).
14. S. Rochat, T.M. Swager, Conjugated amplifying polymers for optical sensing applications, ACS applied materials & interfaces, 5, 4488–4502 (2013).
15. I.A. Terra, R.C. Sanfelice, G.T. Valente, D.S. Correa, Optical sensor based on fluorescent PMMA/PFO electrospun nanofibers for monitoring volatile organic compounds, Journal of Applied Polymer Science, 135, 46128 (2018).
16. T.-Q. Nguyen, V. Doan, B.J. Schwartz, Conjugated polymer aggregates in solution: Control of interchain interactions, The Journal of chemical physics, 110, 4068–4078 (1999).
17. C.-C. Kuo, C.-H. Lin, W.-C. Chen, Morphology and photophysical properties of light-emitting electrospun nanofibers prepared from poly (fluorene) derivative/PMMA blends, Macromolecules, 40, 6959–6966 (2007).
18. I.A. Terra, L.A. Mercante, R.S. Andre, D.S. Correa, Fluorescent and colorimetric electrospun nanofibers for heavy-metal sensing, Biosensors, 7, 61 (2017).
19. K. Tonsomboon, P. Noppakuadrittidej, S. Sutikulsombat, A. Petdum, W. Panchan, N. Wanichacheva, T. Sooksimuang, N. Karoonuthaisiri, Turn-On fluorescence resonance energy transfer (FRET)-based electrospun fibrous membranes: Rapid and ultrasensitive test strips for on-site detection of Mercury (II) ion, Sensors and Actuators B: Chemical, 344, 130212 (2021).
20. J.A. Broussard, B. Rappaz, D.J. Webb, C.M. Brown, Fluorescence resonance energy transfer microscopy as demonstrated by measuring the activation of the serine/threonine kinase Akt, Nature protocols, 8, 265 (2013).
21. J. Choi, W. Lee, B.H. Kim, J. Song, J.-W. Jang, S. Jeon, D.H. Park, Keto-defect induced abnormal exciton behavior in hybrid conjugated polymers, Materials Today Chemistry, 44, 102536 (2025).
22. S. Jo, J. Kim, J. Noh, D. Kim, G. Jang, N. Lee, E. Lee, T.S. Lee, Conjugated polymer dots-on-electrospun fibers as a fluorescent nanofibrous sensor for nerve gas stimulant, ACS applied materials & interfaces, 6, 22884–22893 (2014).
23. K.W. Chew, N.A. Abdul Rahim, P.L. Teh, N.S. Abdul Hisam, S.S. Alias, Thermal degradation of photoluminescence poly (9, 9-dioctylfluorene) solvent-tuned aggregate films, Polymers, 14, 1615 (2022).
24. A.P. Kulkarni, Y. Zhu, S.A. Jenekhe, Quinoxaline-containing polyfluorenes: synthesis, photophysics, and stable blue electroluminescence, Macromolecules, 38, 1553–1563 (2005).
25. Z. Abid, L. Ali, S. Gulzar, F. Wahad, R.S. Ashraf, C.B. Nielsen, Quinoxaline derivatives as

attractive electron-transporting materials, Beilstein Journal of Organic Chemistry, 19, 1694–1712 (2023).
26. Y.-H. Kim, D.-C. Shin, S.H. Kim, C.H. Ko, H.S. Yu, Y.S. Chae, S.-K. Kwon, Novel blue emitting material with high color purity, Advanced Materials, 13, 1690–1693 (2001).
27. A. Satrijo, T.M. Swager, Anthryl-doped conjugated polyelectrolytes as aggregation-based sensors for nonquenching multicationic analytes, Journal of the American Chemical Society, 129, 16020–16028 (2007).
28. S. Jo, D. Kim, S.-H. Son, Y. Kim, T.S. Lee, Conjugated poly (fluorene-quinoxaline) for fluorescence imaging and chemical detection of nerve agents with its paper-based strip, ACS Applied Materials & Interfaces, 6, 1330–1336 (2014).
29. S.A. Jenekhe, J.A. Osaheni, Excimers and exciplexes of conjugated polymers, Science, 265, 765–768 (1994).
30. H.J. Eggimann, F. Le Roux, L.M. Herz, How β-phase content moderates chain conjugation and energy transfer in polyfluorene films, The Journal of Physical Chemistry Letters, 10, 1729–1736 (2019).
31. S. Li, Y. Song, L. Xu, J. Wang, Z. Yang, Y. Zhao, F. Chen, B. Liu, L. Liu, D. Chen, Functional electrospun nanofibrous hybrid materials for colorimetric sensors: a review, ACS omega, 9, 5157–5174 (2024).
32. B. Ding, M. Wang, J. Yu, G. Sun, Gas sensors based on electrospun nanofibers, Sensors, 9, 1609–1624 (2009).
33. A.P. Kulkarni, Y. Zhu, A. Babel, P.-T. Wu, S.A. Jenekhe, New ambipolar organic semiconductors. 2. Effects of electron acceptor strength on intramolecular charge transfer photophysics, highly efficient electroluminescence, and field-effect charge transport of phenoxazine-based Donor− Acceptor materials, Chemistry of Materials, 20, 4212–4223 (2008).
34. T.-Q. Nguyen, I.B. Martini, J. Liu, B.J. Schwartz, Controlling interchain interactions in conjugated polymers: the effects of chain morphology on exciton− exciton annihilation and aggregation in MEH− PPV films, The Journal of Physical Chemistry B, 104, 237–255 (2000).
35. X.-H. Jin, M.B. Price, J.R. Finnegan, C.E. Boott, J.M. Richter, A. Rao, S.M. Menke, R.H. Friend, G.R. Whittell, I. Manners, Long-range exciton transport in conjugated polymer nanofibers prepared by seeded growth, Science, 360, 897–900 (2018).
36. M. Karimi, Diffusion in polymer solids and solutions, Mass transfer in chemical engineering processes, 25, 17 (2011).
37. A. Castel, P. Gutfreund, B. Cabane, Y. Rharbi, Swelling, dewetting and breakup in thin polymer films for cultural heritage, Soft matter, 16, 1485–1497 (2020).
38. Y. Nezili, A. Mdarhri, I. El Aboudi, C. Brosseau, M. Zaghrioui, A. Ghorbal, D. He, J. Bai, Solvent polarity impacts the sorption kinetics and tensile properties of carbon black filled elastomers, Polymer, 264, 125563 (2023).
39. I.Y. Evchuk, R. Musii, R. Makitra, R. Pristanskii, Solubility of polymethyl methacrylate in organic solvents, Russian journal of applied chemistry, 78, 1576–1580 (2005).
40. A. Al-Abduljabbar, I. Farooq, Electrospun polymer nanofibers: processing, properties, and applications, Polymers, 15, 65 (2022).

Supplementary Files

This is a list of supplementary files associated with this preprint. Click to download.

- FinalSupportingInformation.docx